

Dual EKF-Based State and Parameter Estimator for a LiFePO₄ Battery Cell

Danijel Pavković[†], Matija Krznar^{*}, Ante Komljenović^{**}, Mario Hrgetic^{**}, and Davor Zorc^{**}

^{†,**} Faculty of Mechanical Engineering and Naval Architecture, University of Zagreb, Zagreb, Croatia
^{*} Peti Brod Ltd., Zagreb, Croatia

Abstract

This work presents the design of a dual extended Kalman filter (EKF) as a state/parameter estimator suitable for adaptive state-of-charge (SoC) estimation of an automotive lithium-iron-phosphate (LiFePO₄) cell. The design of both estimators is based on an experimentally identified, lumped-parameter equivalent battery electrical circuit model. In the proposed estimation scheme, the parameter estimator has been used to adapt the SoC EKF-based estimator, which may be sensitive to nonlinear map errors of battery parameters. A suitable weighting scheme has also been proposed to achieve a smooth transition between the parameter estimator-based adaptation and internal model within the SoC estimator. The effectiveness of the proposed SoC and parameter estimators, as well as the combined dual estimator, has been verified through computer simulations on the developed battery model subject to New European Driving Cycle (NEDC) related operating regimes.

Key words: Battery, Electric vehicles, Estimation, Kalman filter, Modeling

I. INTRODUCTION

The transportation sector, as the second largest source of CO₂ emissions [1], has a substantial effect on the alarmingly increasing level of greenhouse gases [2]. Moreover, the sensitivity of the automotive/transportation industries to oil prices variability [3] has initiated a gradual shift toward electrified powertrain vehicles, such as plug-in hybrid electric vehicles and battery electric vehicles (BEVs) [1], [3], which are considered to be the key enablers of the more economical and less oil-dependent transport compared to conventional one [3].

However, battery pack size and supporting power electronics systems should be carefully optimized to minimize vehicle electrification and hybridization costs, thereby facilitating a favorable battery range of BEVs and improved fuel efficiency of hybrid electric vehicles (HEVs) [4]. Moreover, to ensure correct battery operation under various operating regimes, the state of charge (SoC) of batteries should be continuously monitored by means of dedicated battery

management system [5], which also needs to provide state-of-health (SoH) monitoring, charge balancing, and thermal management at cell, module, and battery pack level (See [6]-[9] and references therein).

The dynamic model used for battery monitoring is typically nonlinear with respect to SoC and temperature [10]-[15]; thus, a nonlinear or online adaptive estimator may be required for precise SoC estimation over a wide range of battery operating conditions. In references [16] and [17], impedance spectroscopy approach has been used to identify multivariable battery models suitable for utilization within a state estimator, such as the Kalman filter [18]. Comparative reviews presented in [19]-[21] have shown that several other estimator structures may also be suitable for SoC estimation, such as the following:

- 1) a Luenberger estimator, which may be implemented in its basic form or extended by an integral term to improve SoC tracking ability [20];
- 2) a sliding-mode observer, which results in robust estimation in the presence of model uncertainties [22];
- 3) an extended Kalman filter (EKF), which is frequently used for SoC estimation [15], [23]-[25] but may also be prone to model linearization error [26]; and
- 4) a sigma-point Kalman filter [27], unscented Kalman filter [26], [28], or cubature Kalman filter [29], which

Manuscript received Oct. 1, 2016; accepted Jan. 3, 2017

Recommended for publication by Associate Editor Jonghoon Kim.

[†]Corresponding Author: danijel.pavkovic@fsb.hr

Tel: +385-1-6168325, Fax: +385-1-6168351, University of Zagreb

^{*}Peti Brod Ltd., Croatia

^{**}Faculty of Mechanical Engineering and Naval Architecture, University of Zagreb, Croatia

may facilitate improved response speed and SoC tracking accuracy when compared to EKF.

In the above approaches, the SoC estimator design is typically based on the parameter analytical relationships of a priori known (offline identified) battery equivalent model or parameter maps. However, variations in aging and operating conditions (e.g., temperature) variations may affect the accuracy of the battery model within the state estimator, which may, in turn, result in pronounced SoC estimation error. To mitigate the effect of battery model parameter uncertainties to SoC estimation, state estimator may be extended with a parameter estimator utilizing sliding-mode [22] or Kalman filtering [15], [30]-[32] approach, which is then used for state estimator online adaptation. As an additional benefit, monitoring of online battery parameters may also be useful for battery SoH evaluation [14], [31], through monitoring of battery internal resistance [24] or charge capacity [33] with respect to the benchmarks based on battery-accelerated aging tests [34].

This work aims to develop and verify an adaptive SoC estimation framework for a LiFePO₄ battery cell, which might subsequently be extended for battery modules and stacks. For that purpose, the study initially presents the results of experimental characterization and validation of the dynamic model of a state-of-the-art automotive lithium-iron-phosphate (LiFePO₄) battery cell [35]. The proposed equivalent electrical circuit battery model is then used as a basis for the design of a dual EKF adaptive battery SoC estimator, whose parameters can either be supplied by the internal battery model or updated online via dedicated parameter estimator. The effectiveness of the adaptive SoC estimator is verified through simulations based on the experimentally validated LiFePO₄ cell model.

This study is organized as follows: The equivalent electric circuit-based model of LiFePO₄ battery cell and the results of the map identification of battery model parameters are presented in Section II. Section III presents the design of dual Extended Kalman filter (EKF) suitable for battery state and parameter estimation, and the weighting-based method of integration of the battery internal model within the state estimator and the battery parameters identified online. The results of detailed simulation verification of the proposed battery state/parameter estimator are presented in Section IV. Concluding remarks are given in Section V.

II. BATTERY MODELING

This section presents the equivalent electrical circuit-based battery model and the results of experimental characterization of the considered automotive LiFePO₄ cell.

A. Equivalent Circuit Model of the Battery

Fig. 1 shows the considered equivalent electrical circuit

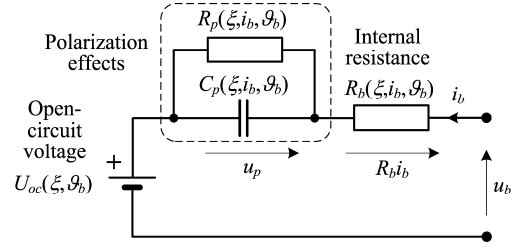


Fig. 1. Quasi-static battery equivalent electrical circuit model.

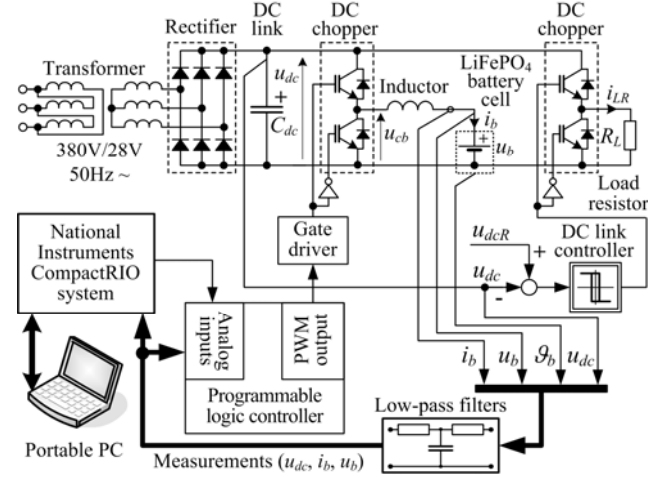


Fig. 2. Principal schematic of battery experimental test bed.

battery model comprising battery series resistance, electrolyte polarization effects, and open-circuit voltage [36]. The model features a voltage source corresponding to the battery open-circuit voltage U_{oc} ; a parallel resistive-capacitive (RC) circuit corresponding to electrolyte polarization effects, and characterized by equivalent polarization resistance R_p and capacitance C_p ; and a series resistor R_b related to battery resistive losses. The above model results in the following voltage u_b versus current i_b relationship in the s -domain ($\tau_p = R_p C_p$ is the polarization time constant):

$$u_b(s) = i_b(s)R_b + \frac{R_p i_b(s)}{\tau_p s + 1} + U_{oc}. \quad (1)$$

In the above battery model, all parameters are dependent on the battery SoC, which is defined as [10]:

$$\xi = 1 - \frac{\Delta Q_b}{Q_{max}(I_b)}, \quad (2)$$

where $\Delta Q_b = -\int i_b dt$ is the overall discharged battery charge, and Q_{max} is the battery charge capacity.

Moreover, the polarization and battery resistive effects are dependent on the battery current and may also exhibit notable dependence on battery operating temperature θ_b , as shown in [10], [11], [13], and [37].

B. Experimental Test Bed of the Battery

The battery model in Fig. 1 is parameterized by recording the model parameter maps for a wide range of battery operating

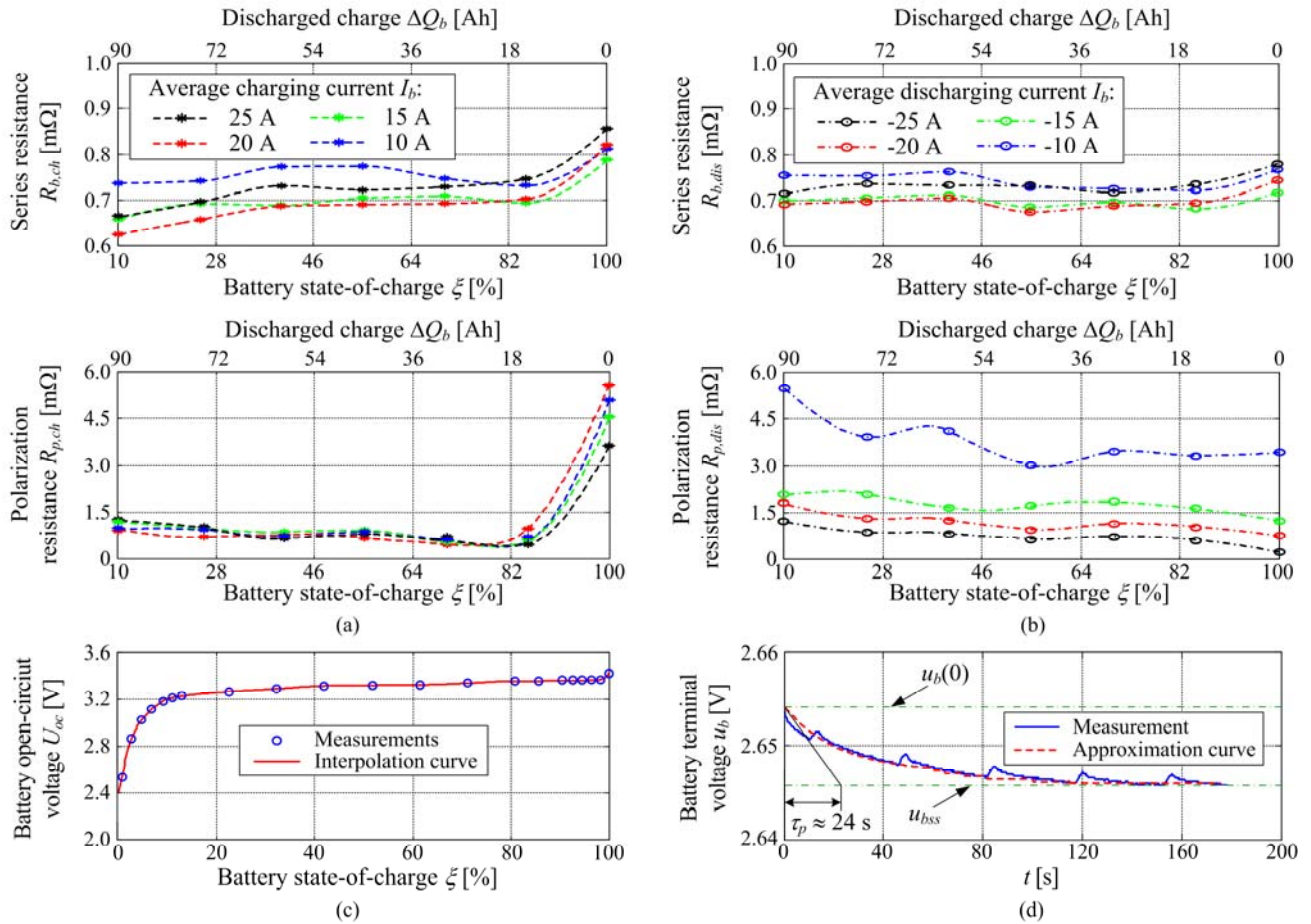


Fig. 3. Experimentally recorded battery internal (series) resistance and polarization resistance maps for charging (a) and discharging (b), open-circuit voltage static curve (c), and characteristic result of constant identification experiment of polarization time (d).

points through an instrumented test bed [38], whose principal schematic is shown in Fig. 2. The battery test setup operation is controlled by the National Instruments CompactRIO data acquisition and control system, which performs the following tasks:

- 1) Collection of battery measurement signals (current i_b , terminal voltage u_b , and operating temperature \mathcal{G}_b) and common direct-current (DC) link voltage u_{dc} of the setup. These signals are low-pass filtered to remove the noise caused by the switching action of the dedicated DC power converter (DC chopper) of the battery.
- 2) Generation of suitable current reference profiles for battery characterization purposes, which are supplied to the low-level current control system implemented on the low-cost programmable logic controller commanding the battery power converter.

The setup also comprises an auxiliary DC chopper, which is used during battery discharging for DC link voltage control through excess DC link energy dissipation at external load resistors.

C. Experimental Characterization Results of the Battery

The experimental characterization procedure, outlined in [39] and [40], has been used to estimate the battery model parameter maps for the considered 3.3 V/100 Ah LiFePO₄ battery cell (type SE100AHA [35]), distinguished by a slightly narrow range of terminal voltage values and extremely low internal resistance. The final battery identification results, obtained over a relatively narrow range of battery temperature \mathcal{G}_b (between 24 °C and 32 °C), are shown in Fig. 3.

Fig. 3(a) and 3(b) show the static maps of the recorded internal resistance $R_b(\xi, i_b)$ and polarization resistance $R_p(\xi, i_b)$. These maps have been reconstructed based on charging/discharging experiments featuring low-magnitude battery current i_b and terminal voltage u_b perturbations with a frequency of 1 Hz, excited under closed-loop control of battery current [39], [40]. The quasi-steady-state portions of the experiments (characterized by negligible dynamic effects of polarization voltage u_p) have been used to fit the internal resistance map data based on a simple battery voltage perturbation model (k , sampling step):

$$\Delta u_b(k) = \Delta i_b(k) R_b(k), \quad (3)$$

where the terminal voltage of the battery and current variations can be expressed through respective time differences:

$$\Delta u_b(k) = u_b(k) - u_b(k-1), \quad (4)$$

$$\Delta i_b(k) = i_b(k) - i_b(k-1). \quad (5)$$

The above model of terminal voltage variations can be rewritten in the form of regression model suitable for parameter estimator design [48]:

$$y(k) = \varphi(k)\theta(k) + e(k), \quad (6)$$

where y is the measurement characterized by Gaussian noise e , φ is a regression variable (regressor), and θ is the parameter to be estimated, treated as a random walk stochastic process:

$$\theta(k) = \theta(k-1) + v(k-1), \quad (7)$$

characterized by a Gaussian perturbation (noise) source v .

The internal resistance estimator has been implemented in the form of Kalman filter, whose design has been presented in [39]; the internal resistance map $R_b(\xi, i_b)$ can be built for the operating points of the selected battery SoC ξ and steady-state battery currents I_b , as shown in Figs. 3(a) and 3(b). Based on the above internal resistance reconstruction, the battery electromotive force can be represented by (Fig. 1):

$$E_b = U_{oc} + u_p = u_b - R_b i_b. \quad (8)$$

Based on this relationship, the steady-state maps of polarization voltage have been obtained by subtracting E_b maps from the open-circuit voltage map $U_{oc}(\xi)$ from Fig. 3(c), which is ultimately used to reconstruct the polarization resistance $R_p(\xi, i_b)$ map points as ratios between the steady-state polarization voltage u_p and the charging/discharging current average value I_b for the particular battery SoC operating point.

The results in Figs. 3(a) and 3(b) show that internal resistance R_b undertakes significantly low values (between 0.62 and 0.85 m Ω), and neither exhibit notable variation with SoC ξ nor significant dissipation with respect to battery current i_b . Conversely, the polarization resistance R_p shows notable increase when the battery is being overcharged (SoC $\xi \rightarrow 1$, Fig. 3(a)) and tends to undertake larger values for lower current values in the case of discharging (Fig. 3(b)).

As expected, the open-circuit voltage curve (Fig. 3(c)) is rather flat over the large range of battery SoC values (as indicated in [35] and [36]). To capture the U_{oc} curve nonlinear trends at fully charged and discharged states, $U_{oc}(\xi)$ points have been collected more densely therein compared to the middle of the operating region.

Fig. 3(d) shows the result of identifying the polarization time constant $\tau_p = R_p C_p$ based on zero-current voltage transient (under “fast” battery current control). The resulting voltage response is then approximated in the least-squares sense by a first-order lag term response [39]:

$$u_b(t) - u_{bss} = (u_b(0) - u_{bss}) \exp(-t/\tau_p), \quad (9)$$

where $u_b(0)$ and u_{bss} are the initial and final battery voltages, respectively (Fig. 3(d)). The polarization time constant does not exhibit notable dissipation with respect to SoC, and its average value $\tau_p = 24$ s (cf. Fig. 3(d)) has been used in the final battery model.

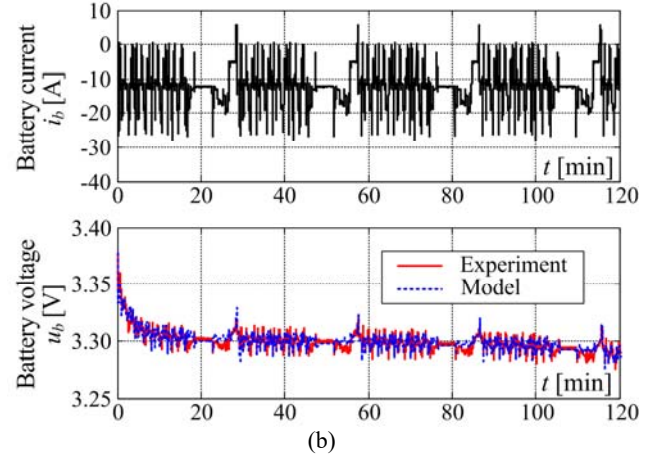
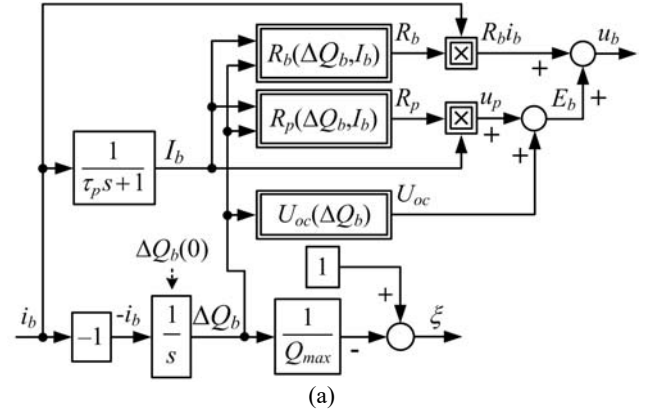


Fig. 4. Battery cell simulation model (a) and results of battery model experimental validation test (b).

Fig. 4(a) shows the block diagram representation of the battery simulation model with battery current as input, where the extracted (discharged) charge ΔQ_b is treated as the model principal state variable, used for battery SoC (ξ) calculation according to Equ. (2). The SoC ξ (discharged charge ΔQ_b) is used alongside the filtered (averaged) battery current value I_b (see Equ. (1)) as input into model static maps $R_b(\Delta Q_b, I_b)$ and $R_p(\Delta Q_b, I_b)$, whereas the open-circuit voltage U_{oc} depends only on ξ (ΔQ_b). The comparative responses of battery simulation model and experimental results are shown in Fig. 4(b) for the case of highly dynamic test profile corresponding to a New European Driving Cycle (NEDC) (cf. e.g., [41]), wherein the model has been implemented within Matlab/Simulink™ using ODE45 numerical integration method with absolute tolerance of 10^{-3} , relative tolerance of 10^{-6} , and minimum integration step of 0.01 s. The particular current demand (current reference) of the battery has been obtained through vehicle simulation model [42], wherein the battery load has been scaled to the single battery cell. The results in Fig. 4(b) indicate that the battery model can track both the quasi-steady-state and transient profiles of the experimentally recorded battery terminal voltage u_b profile. However, a relatively small dynamic error may be present due to measurement quantization error over the slightly narrow cell voltage range (less than 0.1 V) [40].

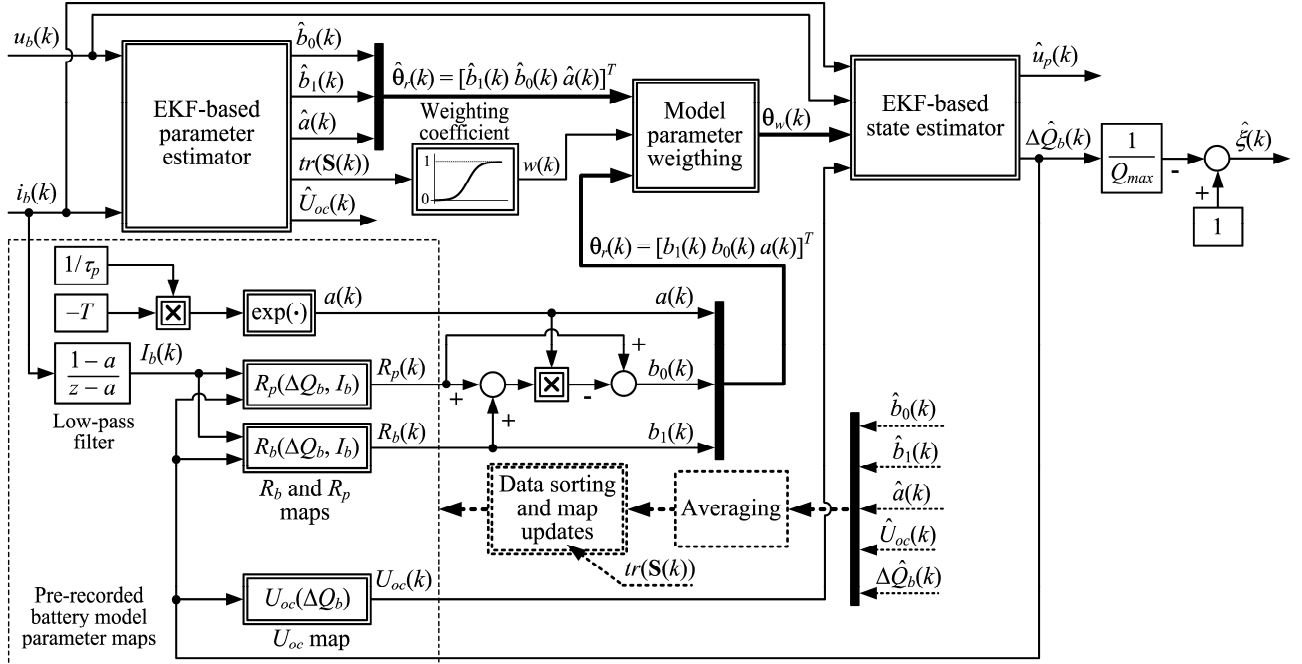


Fig. 5. Principal block diagram representation of the dual EKF-based adaptive SoC estimator.

III. ADAPTIVE SOC ESTIMATOR DESIGN

This section outlines the design of combined state/parameter estimator implemented in the form of a dual EKF for the purpose of adaptive battery SoC estimation.

A. Structure of the Adaptive SoC Estimator

Fig. 5 shows the principal block diagram of the adaptive SoC estimator based on dual EKF. In contrast to [15], [30]–[32], the proposed dual EKF system is arranged so the EKF-based state estimator can utilize either the parameters of the internal nonlinear battery model or those obtained by the second EKF, which estimates the key battery model parameters online.

The parameter estimator accurately estimates the battery model parameters provided that battery measurements i_b and u_b are characterized by sufficient dynamic content (also known as excitation persistence condition) [43]. Otherwise, the parameter estimation should be held, and the state estimator would instead rely on the internal battery model during poor excitation periods (otherwise characterized by estimated parameters drift). A weighting scheme is employed herein based on the error covariance of the parameter estimator used as the measure of external excitation persistence to facilitate a seamless (smooth) transition between the internal model and parameter estimator-supplied battery parameters [43]. The weighting factor used for such “soft” transition between the internal battery model and online parameter estimation is calculated as follows [40]:

$$w = \frac{1 + \tanh(\alpha_1 \cdot tr(\mathbf{S}) + \alpha_0)}{2}, \quad (10)$$

with coefficients α_1 and α_0 chosen empirically based on the properties of matrix trace of the error covariance of the parameter estimator $tr(\mathbf{S})$ (See next section and Appendix).

The parameter maps of the equivalent circuit model of the battery within the state estimator may also be periodically refreshed as updated parameter estimates become available. Thus, the internal model of the battery in Fig. 5 can be adapted with respect to relatively slow temperature variations (which are emphasized for resistance-related parameters R_b and R_p [13], [44]), and even more gradual variations related to battery cycle and calendar life (inevitably affecting all of the parameters of the battery electric circuit [34], [46], [47]). Hence, utilizing battery temperature measurement or estimation [45] and collecting the test results of battery aging [34], [46] may be avoided for parameter map correction. Naturally, precise information about the discharged charge ΔQ_b should also be available for online updates of the parameters of the internal model map, e.g., by using a precise current sensor and charge counting approach (Equ. (2)), while considering the battery Coulombic efficiency [32].

B. Design of the Parameter Estimator

The parameter estimator design is based on the following discrete-time counterpart of the equivalent circuit input–output model of the battery in Equ. (1) [40]:

$$u_b(k) = b_1 i_b(k) + b_0 i_b(k-1) + a u_b(k-1) + (1-a) U_{oc}(k), \quad (11)$$

where $a = \exp(-T/\tau_p)$, $b_1 = R_p$, $b_0 = R_p - a(R_p + R_b)$, and T is the discrete-time model sampling time.

In the battery model in Equ. (11), random variations of the model parameters are again represented by a random walk

stochastic process model [48]:

$$\boldsymbol{\theta}(k) = \boldsymbol{\theta}(k-1) + \mathbf{v}_p(k-1), \quad (12)$$

where $\boldsymbol{\theta} = [b_1 \ b_0 \ a \ U_{oc}]^T$ is the vector of a priori unknown model parameters of the battery, and $\mathbf{v}_p = [v_{b1} \ v_{b0} \ v_a \ v_{Uoc}]^T$ is the vector of independent stochastic Gaussian perturbations in the model parameters, characterized by the diagonal covariance matrix of model perturbations $\mathbf{Q}_p(k) = \text{diag}([q_{b1} \ q_{b0} \ q_a \ q_{Uoc}])$.

Based on Eqs. (11) and (12), the nonlinear relationship of the model output can be redefined in the following form:

$$\begin{aligned} u_b(k) &= \boldsymbol{\chi}(\boldsymbol{\theta}(k), \boldsymbol{\varphi}(k), \eta(k)) \\ &= b_1(k)i_b(k) + b_0(k)i_b(k-1) + a(k)u_b(k-1) \\ &\quad + (1-a(k))U_{oc}(k) + \eta(k), \end{aligned} \quad (13)$$

where $\boldsymbol{\varphi}(k) = [i_b(k) \ i_b(k-1) \ u_b(k-1)]$ represents battery current and voltage measurements arranged in a row vector form, and $\eta(k)$ is the additive Gaussian measurement noise characterized by noise variance $r_p(k)$.

The EKF-based parameter estimator for the above input–output model formulation is provided by [48]:

$$\mathbf{S}(k) = [\mathbf{I} - \mathbf{K}_p(k-1)\mathbf{H}_p(k-1)]\mathbf{S}(k-1) + \mathbf{Q}_p(k-1), \quad (14)$$

$$\mathbf{K}_p(k) = \frac{\mathbf{S}(k)\mathbf{H}_p^T(k)}{\mathbf{H}_p(k)\mathbf{S}(k)\mathbf{H}_p^T(k) + r_p(k)}, \quad (15)$$

$$\hat{\boldsymbol{\theta}}(k) = \hat{\boldsymbol{\theta}}(k-1) + \mathbf{K}_p(k)[u_b(k) - \boldsymbol{\chi}(\boldsymbol{\varphi}(k), \hat{\boldsymbol{\theta}}(k-1), 0)], \quad (16)$$

where \mathbf{I} is the identity matrix, $\mathbf{K}_p(k)$ is the gain matrix of the parameter estimator, and $\mathbf{S}(k)$ is the covariance matrix of the parameter estimation error, whereas $\mathbf{H}_p(k)$ is the gradient of the output of Equ. (16) in the vicinity of estimated parameter vector $\hat{\boldsymbol{\theta}}$:

$$\mathbf{H}_p(k) = \frac{\partial \boldsymbol{\chi}(\boldsymbol{\varphi}(k), \hat{\boldsymbol{\theta}}(k-1), 0)}{\partial \hat{\boldsymbol{\theta}}(k-1)} = [h_{11} \ h_{12} \ h_{13} \ h_{14}], \quad (17)$$

where $h_{11} = i_b(k)$, $h_{12} = i_b(k-1)$, $h_{13} = u_b(k-1) - \hat{U}_{oc}(k-1)$, and $h_{14} = 1 - \hat{a}(k-1)$.

The measurement noise variance r_p can be obtained from the steady-state measurements of the battery voltage; thus, diagonal \mathbf{Q}_p matrix elements represent the estimator-tuning parameters of the EKF-based parameters. Their choice is usually a tradeoff between the tracking ability of parameter variations and noise attenuation.

C. Design of the State Estimator

The battery SoC can be estimated in an open-loop manner based on the battery model alone, such as in [11] and [37]; however, utilizing the state estimator approach offers distinct advantages in terms of (i) the mismatch compensation of the initial condition via state correction feedback and (ii) the ability to tune the estimator response speed and the suppression ability of the measurement noise. In addition, utilizing the Kalman filter-based estimator also provides dynamic estimation error bounds via update of the state error covariance [23].

The design of the state estimator is based herein on the following state–space representation of the equivalent circuit model of the battery (Equ. (1)) and discharged charge within the SoC model (Equ. (2)). The overall model, including stochastic perturbations in system states and measurement (output) noise, is given as follows:

$$\begin{bmatrix} \dot{u}_p \\ \Delta Q_b \end{bmatrix} = \begin{bmatrix} -1/\tau_p & 0 \\ 0 & 0 \end{bmatrix} \begin{bmatrix} u_p \\ \Delta Q_b \end{bmatrix} + \begin{bmatrix} R_p \\ -1 \end{bmatrix} i_b + \begin{bmatrix} v_u \\ v_Q \end{bmatrix}, \quad (18)$$

$$u_b = u_p + U_{oc} + R_b i_b + e, \quad (19)$$

where the stochastic perturbations $\mathbf{v} = [v_u \ v_Q]^T$ in the state vector $\mathbf{x} = [u_p \ \Delta Q_b]^T$ and a scalar noise source e in the battery voltage output equation are assumed to be mutually independent, zero-mean Gaussian processes, and characterized by covariance matrix $\mathbf{Q} = \text{diag}([q_u \ q_Q])$ and variance r , respectively.

The discrete-time counterpart of the above model is provided in the following matrix–vector form:

$$\mathbf{x}(k) = \mathbf{F}(k)\mathbf{x}(k-1) + \mathbf{G}(k)i_b(k-1) + \boldsymbol{\Omega}\mathbf{v}(k-1), \quad (20)$$

$$u_b(k) = \mathbf{h}(\mathbf{x}(k), i_b(k), e(k)), \quad (21)$$

where \mathbf{F} , \mathbf{G} , and $\boldsymbol{\Omega}$ are discrete-time state–space model system, input, and disturbance gain matrix, respectively, defined as:

$$\mathbf{F}(k) = \begin{bmatrix} a(k) & 0 \\ 0 & 1 \end{bmatrix}, \quad \mathbf{G}(k) = \begin{bmatrix} b(k) \\ -T \end{bmatrix}, \quad \boldsymbol{\Omega} = \begin{bmatrix} T & 0 \\ 0 & T \end{bmatrix}, \quad (22)$$

with the coefficient $a(k)$ defined in Equ. (11), and the input matrix \mathbf{G} coefficient $b(k)$ yielded by

$$b(k) = (1-a(k))R_p(k) = b_0(k) + a(k)b_1(k). \quad (23)$$

The latter definition is well suited for the EKF implementation utilizing discrete-time process parameter values obtained from the parameter estimator.

Finally, the vector function of the process output $u_b = \mathbf{h}(\mathbf{x}, i_b, e)$ is given as (note that $R_b = b_1$ in the discrete-time formulation of the process model in Equ. (11))

$$u_b(k) = u_p(k) + U_{oc}(\Delta Q_b(k)) + b_1(k)i_b(k) + e(k). \quad (24)$$

The EKF-based state estimator for the above nonlinear model formulation is defined as [48]

$$\begin{aligned} \hat{\mathbf{x}}(k | k-1) &= \mathbf{F}(k-1)\hat{\mathbf{x}}(k-1 | k-1) \\ &\quad + \mathbf{G}(k-1)i_b(k-1), \end{aligned} \quad (25)$$

$$\begin{aligned} \mathbf{P}(k | k-1) &= \mathbf{F}(k-1)\mathbf{P}(k-1 | k-1)\mathbf{F}^T(k-1) \\ &\quad + \boldsymbol{\Omega}\mathbf{Q}(k-1)\boldsymbol{\Omega}^T, \end{aligned} \quad (26)$$

$$\mathbf{K}(k) = \frac{\mathbf{P}(k | k-1)\mathbf{H}(k)^T}{\mathbf{H}(k)\mathbf{P}(k | k-1)\mathbf{H}(k)^T + r(k)}, \quad (27)$$

$$\mathbf{P}(k | k) = [\mathbf{I} - \mathbf{K}(k)\mathbf{H}(k)]\mathbf{P}(k | k-1), \quad (28)$$

$$\hat{\boldsymbol{\varepsilon}}(k | k-1) = u_b(k) - \mathbf{h}(\hat{\mathbf{x}}(k | k-1), i_b(k), 0), \quad (29)$$

$$\hat{\mathbf{x}}(k | k) = \hat{\mathbf{x}}(k | k-1) + \mathbf{K}(k)\hat{\boldsymbol{\varepsilon}}(k | k-1), \quad (30)$$

where $\hat{\mathbf{x}}(k | k-1)$ and $\hat{\mathbf{x}}(k | k)$ are the a priori and a

posteriori state estimates, respectively; $\hat{\varepsilon}(k|k-1)$ is the estimated a priori prediction error for measurement correction; $\mathbf{P}(k|k-1)$ and $\mathbf{P}(k|k)$ are a priori and a posteriori covariance matrices of the state estimation error, respectively; $\mathbf{K}(k)$ is the EKF estimator gain matrix; $\mathbf{Q}(k-1)$ is the state perturbation covariance matrix; and $\mathbf{H}(k)$ is the gradient of the nonlinear output model with respect to the estimated state \mathbf{x} in the vicinity of the a priori state estimate:

$$\mathbf{H}(k) = \begin{bmatrix} 1 & \frac{\partial U_{oc}(\Delta\hat{Q}_b(k|k-1))}{\partial \Delta\hat{Q}_b(k|k-1)} \end{bmatrix}. \quad (31)$$

Again, the noise variance of the battery voltage (model output) u_b can be determined from steady-state measurements; thus, the covariance matrix \mathbf{Q} becomes the EKF tuning parameter. Its diagonal elements (anticipated-state perturbation variances) are typically chosen as a tradeoff between the estimator tracking ability and suppression of noise in the estimated states.

D. Integration of the State and Parameter Estimators

As illustrated in Fig. 5, the state estimator utilizes the battery model parameters provided by the internal model or dedicated parameter estimator. The accuracy of parameter estimator is affected by the excitation conditions, indicated by the matrix trace of the error covariance of the parameter estimator $tr(\mathbf{S})$ [43]. Hence, more weight should be given to parameter estimates when $tr(\mathbf{S})$ is low, and vice versa, through the weighting function in Equ. (10). The open-circuit voltage characteristic of $U_{oc}(\Delta Q_b)$ is assumed to be changing very slowly (e.g., due to aging [34], [46], [47]); thus, it can be sporadically updated. Conversely, the relatively more pronounced variations of the parameter set $\boldsymbol{\theta}_r = [b_1 \ b_0 \ a]^T$, corresponding to temperature-dependent internal resistance and polarization effects, may be weighed between the internal model and parametric estimation as follows (Fig. 5):

$$\boldsymbol{\theta}_w(k) = w(k)\boldsymbol{\theta}_r(k) + (1-w(k))\hat{\boldsymbol{\theta}}_r(k), \quad (32)$$

where $\boldsymbol{\theta}_r(k)$ and $\hat{\boldsymbol{\theta}}_r(k)$ correspond to parameters obtained from internal model and parameter estimator, respectively.

The above approach results in the following modified forms of EKF-based state estimator (Eqs. (25), (26), and (29)):

$$\hat{\mathbf{x}}(k|k-1) = \tilde{\mathbf{F}}(k-1)\hat{\mathbf{x}}(k-1|k-1) + \tilde{\mathbf{G}}(k-1)i_b(k-1), \quad (33)$$

$$\mathbf{P}(k|k-1) = \tilde{\mathbf{F}}(k-1)\mathbf{P}(k-1|k-1)\tilde{\mathbf{F}}^T(k-1) + \boldsymbol{\Omega}\mathbf{Q}(k-1)\boldsymbol{\Omega}^T, \quad (34)$$

$$\hat{\varepsilon}(k|k-1) = u_b(k) - \tilde{\mathbf{h}}(\hat{\mathbf{x}}(k|k-1), i_b(k), 0), \quad (35)$$

where the modified system and input matrices $\tilde{\mathbf{F}}$ and $\tilde{\mathbf{G}}$, and vector function $\tilde{\mathbf{h}}$ are defined as follows:

$$\tilde{\mathbf{F}}(k) = w(k) \begin{bmatrix} a(k) & 0 \\ 0 & 1 \end{bmatrix} + (1-w(k)) \begin{bmatrix} \hat{a}(k) & 0 \\ 0 & 1 \end{bmatrix}, \quad (36)$$

$$\tilde{\mathbf{G}}(k) = w(k) \begin{bmatrix} b_0(k) + a(k)b_1(k) \\ -T \end{bmatrix} + (1-w(k)) \begin{bmatrix} \hat{b}_0(k) + \hat{a}(k)\hat{b}_1(k) \\ -T \end{bmatrix}, \quad (37)$$

$$\tilde{\mathbf{h}}(\hat{\mathbf{x}}(k|k-1), i_b(k), 0) = U_{oc}(\Delta\hat{Q}_b(k|k-1)) + \hat{u}_p(k|k-1) + [w(k)b_1(k) + (1-w(k))\hat{b}_1(k)]i_b(k). \quad (38)$$

The above result indicates that the proposed weighting scheme results in a single state estimator, whose parameters are seamlessly switched between the internal model and the parameter estimator, further resulting in a smooth gain scheduling-type adaptation of the state and gain update equations and measurement correction update.

IV. SIMULATION RESULTS

The experimentally verified battery simulation model and the proposed dual EKF adaptive SoC estimator for a LiFePO₄ cell have been implemented within Matlab/Simulink software environment. Both estimators have been verified through a realistic simulation scenario corresponding to a battery model subjected to an NEDC driving cycle-based load profile, as illustrated in Section II, and used as the source for state and parameter estimator inputs (measurements).

Fig. 6 shows the results of the non-adaptive EKF-based SoC estimator ($w = 1$) tested during four consecutive NEDC-like battery load cycles (See battery current trace in Fig. 6(a)), with the parameters of EKF-based state estimator listed in the Appendix. The steady-state and dynamic behavior of the EKF-based SoC estimator has been validated for the nominal case, and the cases of notable battery model series resistance R_b and polarization resistance R_p discrepancies (modeling errors) with respect to parameter maps used within the EKF-based SoC estimator:

$$\varepsilon_{R_b} = R_{b,EKF} / R_{b,sim} - 1, \quad (39)$$

$$\varepsilon_{R_p} = R_{p,EKF} / R_{p,sim} - 1, \quad (40)$$

where $R_{b,sim}$ and $R_{p,sim}$ are series and polarization resistance maps used within the battery simulation model, respectively, and $R_{b,EKF}$ and $R_{p,EKF}$ are corresponding maps used within EKF-based state estimator.

The comparative simulation results presented in Figs. 6(b) and 6(c), and the SoC estimation tracking error defined as

$$\Delta\xi(k) = \xi(k) - \hat{\xi}(k), \quad (41)$$

and shown in Fig. 6(d), indicate that polarization and series resistances R_p and R_b mismatch within the estimator may result in notable SoC estimation error when compared to the nominal case (up to 15-fold steady-state error increase). Moreover, the parameter error may result in estimator response slowdown during the initial response transient from the initial condition of the intentionally mismatched estimator state of charge $\xi(0)$

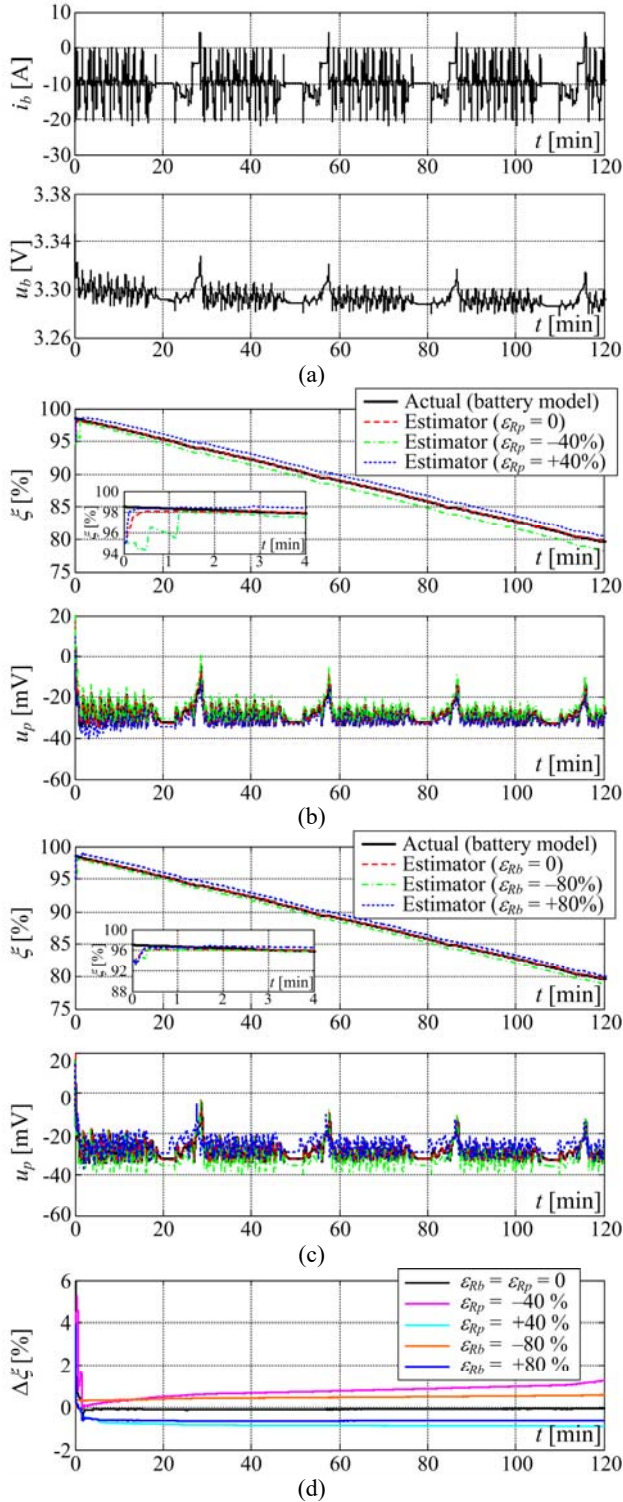


Fig. 6. Results of simulation verification of EKF-based SoC estimator: battery simulation responses (a), estimator responses in presence of R_p error (b) and R_b error (c), and corresponding SoC estimation tracking errors (d).

(See initial response details in Fig. 6(b)). SoC ξ overestimation occurs when the resistance parameters within the estimator are overestimated with respect to the actual battery resistance values R_b and R_p , and vice versa. Conversely, the increase in

polarization resistance R_p within the state estimator tends to produce steady-state overestimation of the polarization voltage according to Equ. (18), whereas the increase in series resistance R_b within the estimator results in the underestimation of the polarization voltage due to the error of the measurement (output) model in Equ. (19) and related correction action according to Eqs. (29) and (30).

Subsequently, an online adaptation based on parameter estimator has been investigated based on the same simulation scenario and for the case of nominal battery model parameters to address the above tracking error problem of state estimator. Fig. 7 shows the results of the proposed EKF-based parameter estimator, whose tuning parameters are also listed in the Appendix, and the corresponding state estimator adapted from the parameter estimator (no reliance on the internal model). The response of the matrix trace of the error covariance of the parameter estimator $tr(S)$ in Fig. 7(a) indicates that battery u_b and i_b measurements in Fig. 6(a) are characterized by substantial periods of favorable excitation (characterized by low $tr(S)$ values), interspersed with intervals of low excitation (indicated by high $tr(S)$ values). The resulting responses of the EKF-based parameter estimator in Fig. 7(a) are characterized by a relatively accurate tracking performance of key battery model parameters R_b , a , b , and U_{oc} (see Eqs. (22)–(24)) during favorable excitation intervals. Conversely, the parameter estimation is stopped (held) during low-excitation periods (i.e., when $tr(S)$ becomes notably larger) to avoid the drift of parameter estimates [43]. The responses of the corresponding adaptive state estimator (dual EKF estimator) are shown in Fig. 7(b). These results indicate that the proposed adaptive state estimation scheme, with state estimator parameter update via parameter estimator alone (corresponding to $w = 0$ case in Eqs. (36)–(38)), can provide estimation accuracies of SoC ξ and the polarization voltage u_p that are comparable to the case of EKF-based state estimator based on internal battery model under nominal conditions (cf. Figs. 7(b) and 6(d)). This finding is also reflected by the traces of the comparative SoC tracking error of the model-based EKF (Fig. 6) and dual-EKF-based adaptive state estimator, as shown in Fig. 7(c). In particular, the SoC error of the adaptive state estimator is remarkably close to the model-based EKF for the nominal case, which indicates accurate capturing of key battery model parameters.

Fig. 8 shows the result of “slow” updates of open-circuit voltage curve $U_{oc}(\xi)$ and the resistance parameter R_b and R_p maps based on parameter estimation and discharged charge from battery model during complete battery discharging under highly dynamic battery load (Fig. 8(a)). The parameter and SoC estimates have been averaged through a low-pass filter with $\Omega_{BW} = 0.04$ rad/s bandwidth to suppress the noise (cf. U_{oc} response in Fig. 7(a)), thereby obtaining smooth parameter map estimates. Fig. 8(b) shows that the resulting $U_{oc}(\xi)$ curve updates (dotted trace in Fig. 8(b)) obtained during favorable excitation conditions of parameter estimator ($tr(S) < 2.5$)

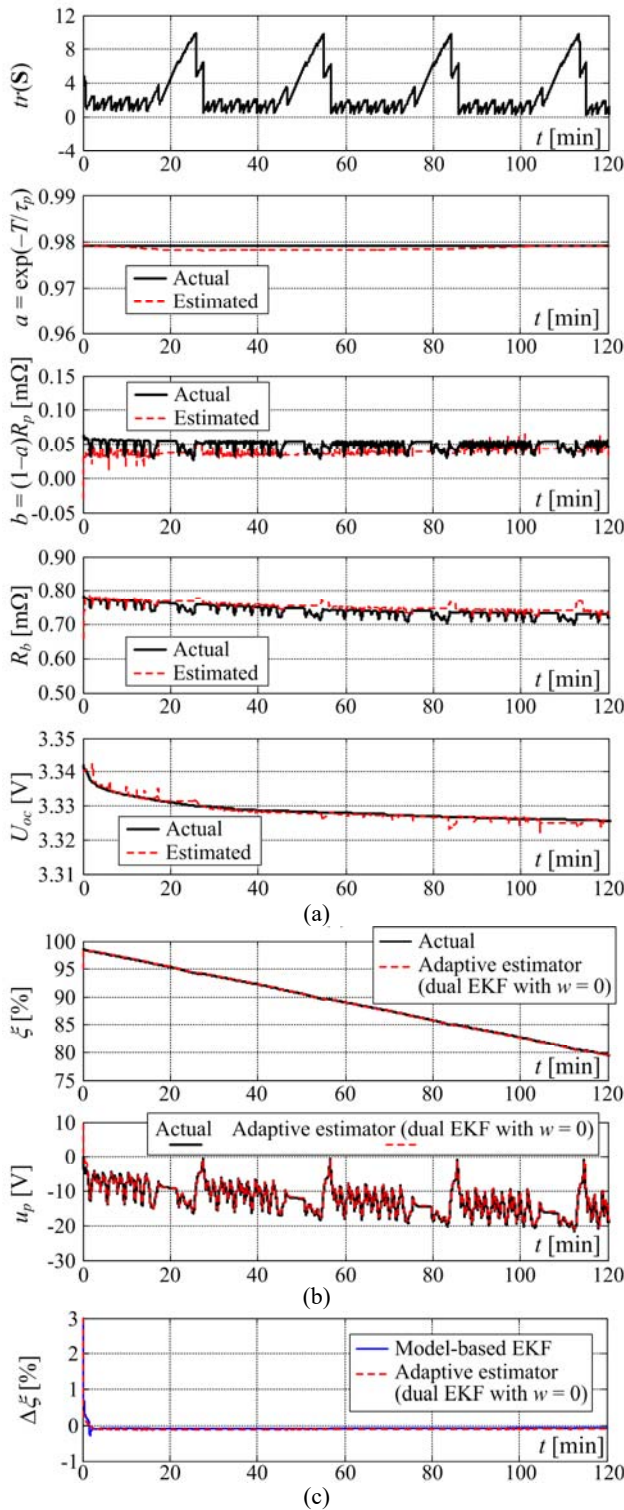


Fig. 7. Results of simulation verification of EKF-based parameter estimator (a), corresponding adaptive state estimator for the case of nominal battery model parameters (b), and comparative SoC tracking error of model-based EKF estimator (c).

indeed match the actual open-circuit voltage map over a wide range of battery SoC. Furthermore, the comparison of actual (battery model) and online reconstructed R_b and R_p maps, shown in Fig. 8(c), also indicate that the proposed algorithm

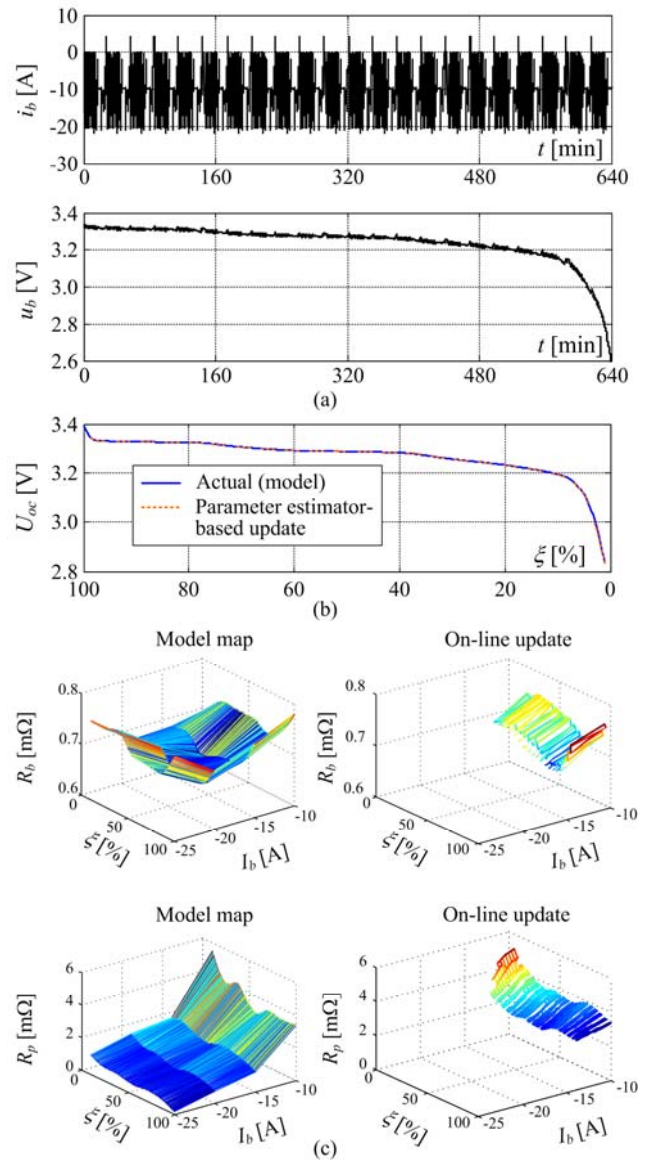


Fig. 8. Battery current and voltage traces during complete discharging (a), and related results of the curve update of the open-circuit voltage (U_{oc}) (b). Comparative assessment of resistance parameter R_b and R_p maps and their online update values (c).

for parameter map update can capture the static map parameter trends for the considered range of battery operation (averaged current ranging from -10 A to -16 A and SoC ranging from 0% to 100% under mostly favorable excitation conditions).

Fig. 9 shows the comparative response of non-adaptive and dual EKF-based adaptive state estimator (state estimator updated from parameter estimator only, $w = 0$) for the case of notable series and polarization resistance mismatch compared to internal model within the non-adaptive state estimator ($\varepsilon_{R_p} = -25\%$ and $\varepsilon_{R_b} = -50\%$). As expected, the non-adaptive state estimator is characterized by a significant SoC tracking error and related polarization voltage steady-state error due to resistance parameter variation. The SoC tracking error is substantially reduced when the parameter estimator is used for

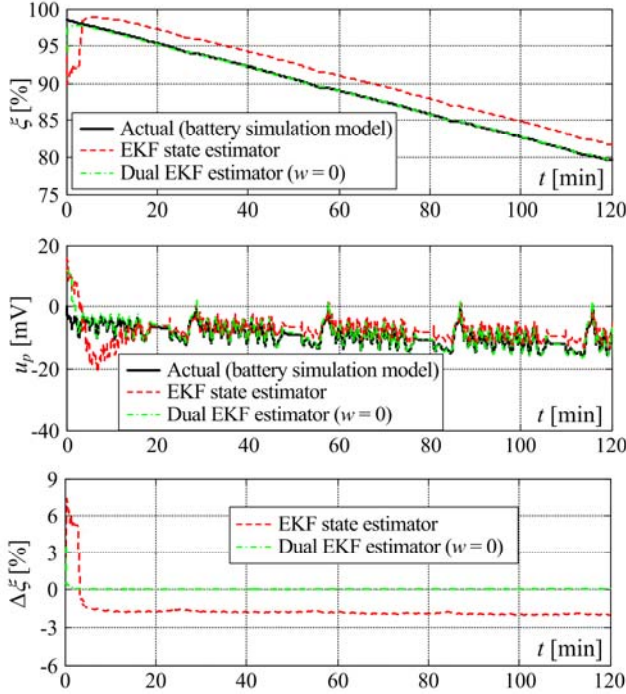


Fig. 9. Comparative responses of non-adaptive and adaptive state estimators updated from the parameter estimator only, subject to the parameter variations of the battery model ($\varepsilon_{R_p} = -25\%$ and $\varepsilon_{R_b} = -50\%$).

online state estimator adaptation.

As discussed in Subsection III. D, the steady-state error of the SoC estimation of the dual EKF-based estimator may be further reduced if state estimator parameters would be provided from the accurate internal model during low-excitation intervals using the proposed parameter weighting scheme in Equ. (32). Figure 10 shows the comparative result of the adaptation scheme of the parameter weighting-based state estimator for the simulation scenario in Fig. 9, assuming that ideal “error-free” battery R_p and R_b parameter maps would be available (i.e., refreshed online beforehand). The weighting scheme responses in Fig. 10(a) confirm that the parameter source is switched from the online parameter estimation to the internal model ($w = 1$) when excitation conditions become unfavorable (i.e., $tr(\mathbf{S})$ becomes large). Once persistent excitation conditions are achieved (i.e., $tr(\mathbf{S})$ is small), the parameter estimator is used instead ($w = 0$). The comparative state estimator responses in Fig. 10(b) show that dual EKF estimator with weighting can indeed improve SoC tracking ability (cf. SoC tracking error $\Delta\xi$ traces in Fig. 10(c) without and with weighting scheme applied).

V. CONCLUSIONS

The work has presented the design of an adaptive battery state estimator based on dual EKF and the formulation of the equivalent electrical circuit battery model, which has been utilized for the estimation of a LiFePO₄ battery cell SoC. The adaptive state estimator features a dedicated EKF-based state

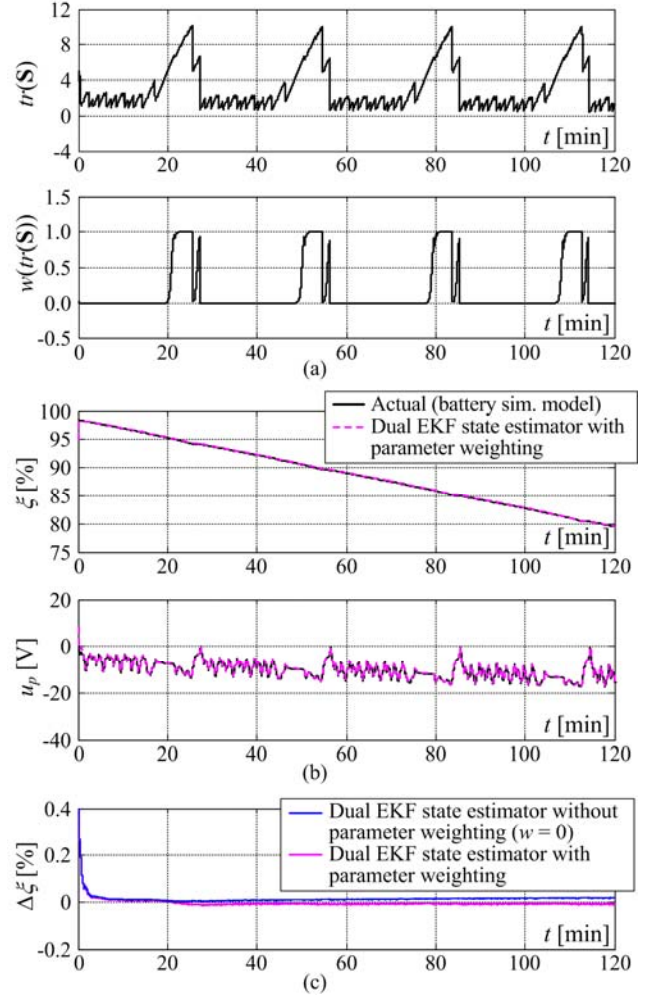


Fig. 10. Responses of the proposed parameter weighting scheme (a), dual EKF-based state estimator with parameter weighting (b), and comparative SoC tracking error without and with parameter weighting (c).

estimator, which may either utilize the internal battery model, characterized by nonlinear parameter maps, or online parameter estimation via the second EKF-based estimator of battery model parameters. To address the persistence excitation issues of the parameter estimator, battery model parameters within the estimator are seamlessly switched between the internal model and online parameter estimation via a simple weighting scheme based on the covariance of the parameter estimator error. Finally, the parameter estimator may also be used to update the internal battery model maps periodically during intervals of favorable excitation.

The effectiveness of the proposed dual EKF-based adaptive SoC estimator has been verified through extensive simulations utilizing experimentally verified LiFePO₄ battery cell model. The results have shown that sensitivity of the EKF-based nonlinear state estimator to battery modeling errors can be successfully mitigated through online parameter estimation and related adaptation of state estimator. The second EKF-based estimator, utilized for that purpose, yields accurate parameter

estimates during conditions of sufficient excitation and can also be used to update battery parameter maps during those intervals. By combining the updated internal model within the state estimator and online parameter estimation via the proposed parameter weighting scheme, the state estimator can achieve additional improvement of the SoC tracking ability compared to utilization of non-updated internal model or online parameter estimation alone. In particular, the updated internal model within the EKF-based state estimator can provide the correct state estimation during battery quasi-steady-state operation (low-excitation conditions), whereas the parameter estimator provides accurate model parameter estimation during highly dynamic operating regimes (characterized by favorable excitation conditions).

Future work may be directed toward the development of SoC estimators for battery modules comprising multiple cells and dedicated battery management system, and SoH estimation based on battery parameter estimator for aging assessment purposes.

APPENDIX

Parameter estimator tuning parameters (Section III.A):

- $T = 0.5$ s
- $r_p = 10^{-4}$
- $q_{b1} = 10^{-5}$
- $q_{b0} = 10^{-5}$
- $q_a = 10^{-5}$
- $q_{Uoc} = 0.01$

State estimator tuning parameters (Section III. B):

- $T = 0.5$ s
- $r = 10^{-4}$
- $q_u = 3 \cdot 10^{-4}$
- $q_Q = 0.03$

Tuning parameters of weighting function in Equ. (10):

- $\alpha_1 = 2$
- $\alpha_0 = -12$

ACKNOWLEDGMENT

This work is supported by the Croatian Science Foundation (HRZZ) through the "Optimization of renewable electricity generation systems connected in a microgrid" grant (No. 08/40), with the research also being conducted within the activities of the Center of Research Excellence for Data Science and Cooperative Systems supported by the Ministry of Science, Education, and Sports of the Republic of Croatia.

REFERENCES

- [1] A. Y. Saber and G. K. Venayagamoorthy, "Plug-in vehicles and renewable energy sources for cost and emission reductions," *IEEE Trans. Ind. Electron.*, Vol. 58, No. 4, pp. 1229-1238, Apr. 2011.
- [2] J. Hansen, M. Sato, P. Kharecha, D. Beerling, R. Berner, V. Masson-Delmotte, M. Pagani, M. Raymo, D. L. Royer, and J. Zachos, "Target atmospheric CO₂: Where should humanity aim?," *The Open Atmospheric Science Journal*, Vol. 2, pp. 217-231, Nov. 2008.
- [3] A. Poullikkas, "Sustainable options for electric vehicle technologies," *Renewable and Sustainable Energy Reviews*, Vol. 41, pp. 1277-1287, Jan. 2015.
- [4] International Renewable Energy Agency (IRENA): "Road Transport: The Cost of Renewable Solutions," IRENA's Costing Study (<http://www.irena.org/publications>), 2013.
- [5] H. Rahimi-Eichi, U. Ojha, F. Baronti, and M.-Y. Chow: "Battery management system – An overview of its application in the smart grid and electric vehicles," *IEEE Ind. Electron. Mag.*, Vol. 7, No 2, pp. 5-16, Jun. 2013.
- [6] J. Cao and A. Emadi: "Batteries need electronics - Battery management systems vary according to chemistry and applications," *IEEE Ind. Electron. Mag.*, Vol. 5, No 1, pp. 27-35, Mar. 2011.
- [7] K. W. E. Cheng, B. P. Divakar, H. Wu, K. Dong, and H. F. Ho, "Battery-management system (BMS) and SoC development for electric vehicles," *IEEE Trans. Veh. Technol.*, Vol. 60, No. 1, pp. 76-88, Jan. 2011.
- [8] M. Einhorn, W. Roessler, and J. Fleig, "Improved performance of serially connected Li-Ion batteries with active cell balancing in electric vehicles," *IEEE Trans. Veh. Technol.*, Vol. 60, No. 6, pp. 2448-2457, Jul. 2011.
- [9] L. Y. Wang, M. P. Polis, G. G. Yin, W. Chen, Y. Fu, and C. C. Mi, "Battery cell identification and SoC estimation using string terminal voltage measurements," *IEEE Trans. Veh. Technol.*, Vol. 61, No. 7, pp. 2925-2935, Sep. 2012.
- [10] M. Ceraolo, "New dynamical models of lead-acid batteries," *IEEE Trans. Power Syst.*, Vol. 15, No. 4, pp. 1184-1190, Nov. 2000.
- [11] N. A. Windarko and J. Choi, "SoC estimation based on OCV for NiMH batteries using and improved takacs model," *Journal of Power Electronics*, Vol. 10, No. 2, pp. 181-186, Mar. 2010.
- [12] D.-H. Shin, J.-B. Jeong, T.-H. kim, and H.-J. Kim, "Modeling of lithium battery cells for plug-in hybrid vehicles," *Journal of Power Electronics*, Vol. 13, No. 3, pp. 429-436, May 2013.
- [13] K. Uddin, A. Picarelli, C. Lynes, N. Taylor, and J. Marco, "An acausal Li-Ion battery pack model for automotive applications," *Energies*, Vol. 7, pp. 5675-5700, Sep. 2014.
- [14] J. Remmlinger, M. Buchholz, M. Meiler, P. Bernreuter, and K. Dietmayer, "State-of-health monitoring of lithium-ion batteries in electric vehicles by on-board internal resistance estimation," *Journal of Power Sources*, Vol. 196, No. 12, pp. 5357-5363, Jun. 2011.
- [15] M. Mastali, J. Vasquez-Arenas, R. Fraser, M. Fowler, S. Afshar, and M. Stevens, "Battery state of charge estimation using Kalman filtering," *Journal of Power Sources*, Vol. 239, pp. 294-307, Oct. 2013.
- [16] D. Andre, M. Meiler, K. Steiner, C. Wimmer, T. Soczka-Guth, and D. U. Sauer, "Characterization of high-power lithium-ion batteries by electrochemical impedance spectroscopy. II. Modelling," *Journal of Power Sources*, Vol. 196, No. 12, pp. 5349-5356, Jun. 2011.
- [17] J.-H. Lee and W. Choi, "Novel state-of-charge estimation method for lithium polymer batteries using electrochemical impedance spectroscopy," *Journal of Power Electronics*, Vol. 11, No. 2, pp. 237-243, Mar. 2011.
- [18] J. Xu, C. C. Mi, B. Cao, and J. Cao, "A new method to estimate the state of charge of lithium-ion batteries based

- on the battery impedance model,” *Journal of Power Sources*, Vol. 233, pp. 277-284, Jul. 2013.
- [19] J. Li, J. K. Barillas, C. Guenther, and M. A. Danzer, “A comparative study of state of charge estimation algorithms for LiFePO₄ batteries used in electric vehicles,” *Journal of Power Sources*, Vol. 230, pp. 244-250, May 2013.
- [20] Z. Zou, J. Hu, C. Mi, B. Cao, and Z. Chen, “Evaluation of model based state of charge estimation methods for lithium-ion batteries,” *Energies*, Vol. 7, pp. 5065-5082, Aug. 2014.
- [21] W.-Y. Chang, “The state of charge estimating methods for battery: A review,” *ISRN Applied Mathematics*, Vol. 2013, Article ID 956792, 7 pages, 2013.
- [22] S. Dey, S. Mohon, P. Pisu, B. Ayalew, and S. Onori, “Online state and parameter estimation of battery-double layer capacitor hybrid energy storage system,” in *Proceedings of IEEE 54th Annual Conference on Decision and Control (CDC 2015)*, pp. 676-681, 2015.
- [23] G. L. Plett, “Extended Kalman filtering for battery management systems of LiPB-based HEV battery packs – Part 3, state and parameter estimation,” *Journal of Power Sources*, Vol. 134, No. 2, pp. 277-262, Aug. 2004.
- [24] J. Kim and B. H. Cho, “State-of-charge estimation and state-of-health prediction of a Li-ion degraded battery based on an EKF combined with a per-unit system,” *IEEE Trans. Veh. Technol.*, Vol. 60, No. 9, pp. 4249-4260, Nov. 2011.
- [25] M. Charkhgard and M. Farrokhi, “State of charge estimation for lithium-ion batteries using neural networks and EKF,” *IEEE Trans. Ind. Electron.*, Vol. 57, No. 12, pp. 4178-4187, Dec. 2010.
- [26] J. Zhang and C. Xia, “State-of-charge estimation of valve regulated lead acid battery based on multi-state Unscented Kalman Filter,” *Electrical Power and Energy Systems*, Vol. 33, pp. 472-476, Mar. 2011.
- [27] B.-H. Seo, T. H. Nguyen, D.-C. Lee, K.-B. Lee, and J.-M. Kim, “Condition monitoring of lithium polymer batteries based on sigma-point Kalman filter,” *Journal of Power Electronics*, Vol. 12, No. 5, pp. 778-786, Sep. 2012.
- [28] W. He, N. Willard, C. Chen, and M. Pecht, “State of charge estimation for electric vehicle batteries using unscented Kalman filtering,” *Microelectronics Reliability*, Vol. 53, pp. 840-847, Jun. 2013.
- [29] B. Xia, H. Wang, Y. Tian, M. Wang, W. Sun, and Z. Hu, “State of charge estimation of lithium-ion batteries using an adaptive cubature Kalman filter,” *Energies*, Vol. 8, pp. 5919-5936, Jun. 2015.
- [30] L. Pei, C. Zhu, T. Wang, R. Lu, and C. C. Chan, “Online peak power prediction based on a parameter and state estimator for lithium-ion batteries in electric vehicles,” *Energy*, Vol. 66, pp. 766-778, Mar. 2014.
- [31] J. Kim, S. Lee, and B. H. Cho, “Complementary cooperation algorithm based on DEKF combined with pattern recognition for SoC/Capacity estimation and SoH prediction,” *IEEE Trans. Power Electron.*, Vol. 27, No. 1, pp. 436-451, Jan. 2012.
- [32] J. Wang, B. Cao, Q. Chen, and F. Wang, “Combined state of charge estimator for electric vehicle battery pack,” *Control Engineering Practice*, Vol. 15, No. 12, pp. 1569-1576, Dec. 2007.
- [33] M. Shahriari and M. Farrokhi, “Online state-of-health estimation of VRLA batteries using state-of-charge,” *IEEE Trans. Ind. Electron.*, Vol. 60, No. 1, pp. 191-202, Jan. 2013.
- [34] N. Omar, M. A. Monem, Y. Firouz, J. Salminen, J. Smekens, O. Hegazy, H. Gaulous, G. Mulder, P. Van den Bossche, T. Coosemans, and J. Van Mierlo, “Lithium iron phosphate based battery – Assessment of aging parameters and development of life cycle model,” *Applied Energy*, Vol. 113, pp. 1575-1585, Jan. 2014.
- [35] GWL/Power Group, “SE100AHA cell specification,” (<http://www.ev-power.eu/CALB-40Ah-400Ah/SE100AHA-Lithium-Cell-LiFePO4-3-2V-100Ah.html>), 2015.
- [36] M. A. Roscher and D. U. Sauer, “Dynamic electric behavior and open-circuit-voltage modeling of LiFePO₄-based lithium-ion secondary batteries,” *Journal of Power Sources*, Vol. 196, No. 1, pp. 331-336, Jan. 2011.
- [37] M. Chen and G.-A. Rincón-Mora, “Accurate electrical battery model capable of predicting runtime and I-V performance,” *IEEE Transactions on Energy Conversion*, Vol. 21, No. 2, pp. 504-511, Jun. 2006.
- [38] D. Pavković, M. Hrgetić, A. Komljenović, A. Lisac, and J. Deur, “Battery/ultracapacitor test setup control system design and verification,” in *Proc. of IEEE EUROCON 2013*, pp. 1050-1057, 2013.
- [39] D. Pavković, A. Komljenović, and M. Hrgetić, “Control-oriented modeling and experimental identification of a VRLA battery,” in *Proc. of 17th International Conference on Electrical Drives and Power Electronics (EDPE 2013)*, pp. 2-9, 2013.
- [40] D. Pavković, A. Komljenović, M. Hrgetić, and M. Krznar, “Experimental characterization and development of a SoC/SoH estimator for a LiFePO₄ battery cell,” in *Proc. of IEEE EUROCON 2015*, pp. 397-402, 2015.
- [41] US Environmental Protection Agency, “Dynamometer drive schedules” (<http://www.epa.gov/nvfel/testing/dynamometer.htm>), Jul. 2014.
- [42] D. Pavković, M. Lobrović, M. Hrgetić, and A. Komljenović, “A design of DC bus control system for EVs based on battery/ultracapacitor hybrid energy storage,” in *Proc. of 2014 IEEE International Electrical Vehicle Conference (IEVC 2014)*, 2014.
- [43] L. Ljung, *System Identification – Theory for the User*, Prentice-Hall Inc., 1987, Chap. 14.
- [44] C. Anatolae, J. Marco, and F. Assadian, “A novel method for the parameterization of a Li-Ion cell model for EV/HEV control applications,” *IEEE Trans. Veh. Technol.*, Vol. 61, No. 9, pp. 3881-3892, Nov. 2012.
- [45] J. Sun, G. Wei, L. Pei, R. Lu, K. Song, C. Wu, and C. Zhu, “Online internal temperature estimation for lithium-ion batteries based on Kalman filter,” *Energies*, Vol. 8, pp. 4400-4415, May 2015.
- [46] S. B. Peterson, J. Apt, and j. F. Whitacre, “Lithium-ion battery cell degradation resulting from realistic vehicle and vehicle-to-grid utilization,” *Journal of Power Sources*, Vol. 195, pp. 2385-2392, Apr. 2010.
- [47] M. Ecker, J. B. Gerschler, J. Vogel, S. Käbitz, F. Hust, P. Dechent, and D. U. Sauer, “Development of a lifetime prediction model for lithium-ion batteries based on extended accelerated aging test data,” *Journal of Power Sources*, Vol. 215, pp. 248-257, Oct. 2012.
- [48] M. S. Grewal and A. P. Andrews, *Kalman Filtering – Theory and Practice*, John Wiley and Sons Ltd., 2001, Chap. 5.



Danijel Pavković (b. 1975 in Croatia) received his B.Sc. and M.Sc. degrees in Electrical Engineering in 1998 and 2003, respectively, and his Ph.D. degree in Mechanical Engineering in 2007, all from the University of Zagreb, Croatia. Since 2016, he has held the position of an Associate Professor

at the Faculty of Mechanical Engineering and Naval Architecture of the University of Zagreb, where he teaches subjects in electrical machines, electrical servo drive control, and digital control systems. He has participated in 18 research and development projects supported by the Ministry of Science, Education, and Sport of the Republic of Croatia, the Ford Motor Company, Jaguar Cars Ltd., CROSCO Integrated Drilling & Well Services Company, European Commission (7th Framework Program, FP7), Croatian Science Foundation, and Croatian Agency for SMEs, Innovations, and Investments (HAMAG-BICRO). His research interests include modeling, estimation, and control of battery and ultracapacitor energy storage systems, and power converters in microgrids, electrical servo drives with application in oil-drilling system retrofitting, and adaptive control of vehicle mechatronic systems.



Matija Krznar (b. 1987 in Croatia) received his B.Eng. and M.Eng. degrees in Mechanical Engineering in 2009 and 2010, respectively, from the University of Zagreb, Croatia. He is currently a Ph.D. student at University of Zagreb, Faculty of Mechanical Engineering and Naval Architecture, Automation Department. His main interests are control algorithms, mathematical modeling, simulation of real-time systems, multirotor flying vehicles, and software/hardware integration. He is volunteering as an instructor at ZIRK Robotics Club, Sveti Kriz Zacetje, lecturing in mBot (Arduino, Scratch platform) and Arduino/Raspberry.



Ante Komljenović (b. 1987 in Croatia) received his M.Eng. degree in Mechanical Engineering in 2013 from the Faculty of Mechanical Engineering and Naval Architecture, University of Zagreb, Croatia. Since 2013, he has been a department assistant at the Faculty of Mechanical Engineering and Naval Architecture of the University of Zagreb, where he participates on research and development projects supported by the Ford Motor Company and European Commission (within Horizon 2020 Framework). His research interests include estimation and control of battery and ultracapacitor energy storage systems.



Mario Hrgetić (b. 1979 in Croatia) received his B.Sc. and Ph.D. degrees in Electrical Engineering in 2004 and 2015, respectively, both from the Faculty of Electrical Engineering and Computing of the University of Zagreb, Croatia. Since December 2005, he has been employed as the research and teaching assistant at the Faculty of Mechanical Engineering and Naval Architecture, University of Zagreb, where he participates in research and teaching activities in the field of electrical engineering, electronics, and sensors. He has participated in numerous research and development projects supported by the Ministry of Science, Education, and Sports of the Republic of Croatia, University of Zagreb, the Ford Motor Company, Jaguar Cars Ltd., European Commission (FP7), and Croatian Science Foundation. His research interests include development of the estimators based on the sensor fusion methodology with applications on vehicle dynamics and automotive mechatronic systems, modeling of DC/DC power converters with applications to battery and ultracapacitor energy storage systems, and design of instrumentation systems.



Davor Zorc (b. 1954 in Zagreb, Croatia) received his B.Sc., M.Sc., and Ph.D. degrees in electrical engineering in 1978., 1986, and 1990, all from the University of Zagreb, Faculty of Electrical Engineering and Computing. From 1978 to 1982, he has been employed as a development engineer in industrial electronics institute "Končar," where he designed electronic control and measurement equipment. In 1982, he joined the Faculty of Mechanical and Naval Engineering, University of Zagreb, where he is currently employed as a full-time professor and teaches subjects in electrical engineering, electronics, and microprocessor-based control systems. In 1987, he was granted a research scholarship at Florida State University, Tallahassee, Florida. He has conducted research in parallel decomposition of control algorithms. His main research interests include computer control and robots, parallel processing, and computerized instrumentation systems.